

# Improving LMA predictions with non-standard interactions: neutrino decay in solar matter?

C. R. Das\*, João Pulido†

*CENTRO DE FÍSICA TEÓRICA DE PARTÍCULAS (CFTP)*

*Departamento de Física, Instituto Superior Técnico*

*Av. Rovisco Pais, P-1049-001 Lisboa, Portugal*

## Abstract

It has been known for some time that the well established LMA solution to the observed solar neutrino deficit fails to predict a flat energy spectrum for SuperKamiokande as opposed to what the data indicates. It also leads to a Chlorine rate which appears to be too high as compared to the data. We investigate the possible solution to these inconsistencies with non standard neutrino interactions, assuming that they come as extra contributions to the  $\nu_\alpha\nu_\beta$  and  $\nu_\alpha e$  vertices that affect both the propagation of neutrinos in the sun and their detection. We find that, among the many possibilities for non standard couplings, only the diagonal imaginary ones lead to a solution to the tension between the LMA predictions and the data, implying neutrino instability in the solar matter. Unitarity requirements further restrict the solution and a neutrino decay into an antineutrino and a majoron within the sun is the one favoured. Antineutrino probability is however too small to open the possibility of experimentally observing antineutrinos from the sun due to NSI.

---

\*E-mail: crdas@cftp.ist.utl.pt

†E-mail: pulido@cftp.ist.utl.pt

# 1 Introduction

Neutrino non-standard interactions (NSI) have been introduced long ago [1, 2] to account for a possible alternative solution to the solar neutrino problem. Since then a great deal of effort has been dedicated to study its possible consequences. To this end possible NSI signatures in neutrino processes have been investigated, models for neutrino NSI have been developed and bounds have been derived [3–17]. Specific investigations of NSI in matter have also been performed within the context of supernova [18] and solar neutrinos [19–24].

Although LMA is generally accepted as the dominant solution to the solar neutrino problem [25, 26], not only its robustness has been challenged by NSI, as it can shift the LMA solution to the dark side region of parameter space [22], but also some inconsistencies remain regarding its agreement with the data [27, 28]. In fact, while the SuperKamiokande (SK) energy spectrum appears to be flat [29, 30], the LMA prediction shows a clear negative slope in the same energy range. With the expected improvement in the trigger efficiency for threshold electron energies as low as 3 MeV to be reached in the near future [31], such a disagreement, if it persists, may become critical. Moreover the LMA solution predicts an event rate for the Cl experiment [32] which is  $2\sigma$  above the observed one [33]. These are motivations to consider ‘beyond LMA’ solar neutrino solutions in which NSI may play a subdominant, although important role.

In order for NSI to be detectable and therefore relevant in physical processes, the characteristic scale of the new physics must not be too much higher than the scale of the physics giving rise to the Standard Model interactions,  $\Lambda_{EW} \simeq G_F^{-1/2}$ . Possible realisations are one loop radiative models of Majorana neutrino mass [34], supersymmetric SO(10) with broken D-parity [35], the inverse seesaw in a supersymmetry context [36] or triplet seesaw models [37]. Since the scale at which the new interaction arises is supposed to be not too far from the electroweak scale, its coupling may be parameterised by  $G_F \varepsilon$  where  $\varepsilon \simeq \Lambda_{EW}^2 / \Lambda_{NP}^2 \simeq 10^{-2}$  for d=6 or  $\varepsilon \simeq \Lambda_{EW}^4 / \Lambda_{NP}^4 \simeq 10^{-4}$  for d=8 operators respectively. For type I seesaw, NSI are of course negligible.

In this paper we will be concerned with NSI both at the level of propagation through solar matter and at the level of detection. Matter NSI are defined through the addition of an effective operator to the Lagrangian density

$$\mathcal{L}_{NSI}^M = -2\sqrt{2}G_F \varepsilon_{\alpha\beta}^{fP} [\bar{f}\gamma^\mu P f][\bar{\nu}_\alpha \gamma_\mu P_L \nu_\beta] \quad (1)$$

where  $f = e, u, d$ ,  $P$  denotes the projection operator for left and right chirality and  $\varepsilon_{\alpha\beta}^{fP}$  parameterizes the deviation from the standard interactions. At present there is no evidence at all of such operators generated at a scale  $\Lambda_{NP}$ , hence the variety of theoretical models for the physics accessible to the LHC.

There are several ways to introduce NSI. For instance in fermionic seesaw models, once the heavy fermions (singlets or triplets) are integrated out, modified couplings of leptons to gauge bosons are obtained in the form of a non-unitary leptonic matrix. The strong bounds on the deviation from the unitarity of this matrix constrain these NSI to be  $\lesssim O(10^{-3})$  [13].

Alternatively NSI can be generated by other new physics above the electroweak scale not related to neutrino masses. As a consequence an SU(2) gauge invariant formulation of NSI is required, since any gauge theory beyond the standard model must necessarily respect its gauge symmetry. Strong bounds from four charged fermionic processes [38] and electroweak precision tests requiring fine tunings imply that possibilities are limited for such scenarios [14, 39]. Another way to introduce NSI is by assuming that there are extra contributions to the vertices  $\nu_\alpha\nu_\beta$  and  $\nu_\alpha e$ . In such a case the parameters  $\varepsilon_{\alpha\beta}$  describe the deviation from the standard model vertices and are treated like the standard interactions. It is possible that other effects are present in this case that depend on the nature and number of particles that may be introduced in a particular model. We adopt this procedure in the present paper and assume these model dependent effects to be negligible.

The paper is organized as follows: section 2 is devoted to the study of the propagation and detection of solar neutrinos. We start by reviewing the derivation of the neutrino refraction indexes with standard interactions (SI) and their generalization to NSI in order to obtain the matter Hamiltonian. The survival and conversion probabilities to  $\nu_\mu$  and  $\nu_\tau$  are then evaluated through the numerical integration of the Schrödinger like equation using the Runge-Kutta method and the experimental event rates are obtained. We use the reference solar model with high metallicity, BPS08(GS) [40]. In section 3 we investigate the influence of the NSI couplings on these rates in order to find whether and how the fits can be improved with respect to the LMA ones. We concentrate in particular on the elimination of the upturn in the SuperKamiokande spectrum predicted by LMA for energies below 8-10 MeV not supported by the data [27–30] and on the Chlorine rate whose LMA prediction exceeds the data by  $2\sigma$  [32, 33]. We find the intriguing result that only imaginary diagonal couplings in the matter Hamiltonian provide a suitable solution to the problem. In fact all other possibilities, namely imaginary off diagonal couplings or real couplings, either diagonal or off diagonal, are unable to change the LMA solution. This means that eliminating the tension with the data implies complex matter Hamiltonian eigenvalues and therefore neutrino decay induced by the solar matter. In section 4 it will be seen that the condition of consistency with the data on the event rates is not sufficient, owing to the requirement of unitarity which severely restricts the correct solution. Furthermore, the neutrino decay in the sun suggested long ago into an antineutrino and a scalar particle (majoron) [41–44] is the favoured channel. In section 5 we present a brief discussion and summarize our main conclusions.

## 2 Interaction potentials, the Hamiltonian and the rates

In this section we develop the framework that will be used as the starting point for the analysis of the NSI couplings in section 3. To this end we review the derivation of the neutrino interaction potentials in solar matter, its generalization to non standard interactions along with the corresponding matter Hamiltonian and the event rates.

## 2.1 Interaction potentials and the Hamiltonian

While  $\nu_e$ 's propagate through solar matter their interaction with electrons proceeds both through charged and neutral currents (CC) and (NC). Recalling that for standard interactions (SI) each tree level vertex accounts for a factor

$$\frac{g_L}{\cos\theta_W}(T_{3L} - 2Q_f \sin^2\theta_W), \quad (2)$$

inserting the W, Z propagators and the electron external lines, one gets for the  $\nu_e$  interaction potentials

$$(V_e)_{CC} = G_F\sqrt{2}N_e, \quad (V_e)_{NC} = G_F/\sqrt{2}(-1 + 4\sin^2\theta_W)N_e \quad (3)$$

where  $G_F$  is the Fermi constant,  $G_F/\sqrt{2} = g_L^2/8m_W^2$ . For the interactions with quarks only neutral currents are involved and the additivity of the quark-current vertices gives for protons

$$V_p = (V_p)_{NC} = G_F/\sqrt{2}(1 - 4\sin^2\theta_W)N_e \quad (4)$$

and for neutrons

$$V_n = (V_n)_{NC} = -G_F/\sqrt{2}N_n. \quad (5)$$

Hence the neutrino interaction potential is for standard interactions<sup>1</sup>

$$V(SI) = V_e + V_p + V_n = G_F\sqrt{2}N_e \left(1 - \frac{N_n}{2N_e}\right) = V_c + V_n \quad (6)$$

with  $V_e = (V_e)_{CC} + (V_e)_{NC}$  and  $V_c = V_e + V_p = G_F\sqrt{2}N_e$ .

In order to introduce NSI we assume that each diagram associated to neutrino propagation in matter (i.e. CC and NC currents in  $\nu_\alpha e^-$  and NC currents in  $\nu_\alpha u$ ,  $\nu_\alpha d$  scattering) is multiplied by a factor  $\varepsilon_{\alpha\beta}^{e,u,d}{}^P$  parameterising the deviation from the standard model. So we assume that the interaction potential for  $\nu_\alpha$  ( $\alpha = e, \mu, \tau$ ) on electrons involves both CC and NC giving rise to possible lepton flavour violation:  $\nu_\alpha$  for  $\alpha \neq e$  may have CC. So for the charged current of  $\nu_e$  with electrons we have

$$(V_e)_{CC}(NSI) = \frac{g_L^2}{2m_W^2}(\varepsilon_{\alpha\beta}^{eP})_{CC}N_e \quad (7)$$

and for the neutral current

$$(V_e)_{NC}(NSI) = \frac{g_L^2}{4m_W^2}(-1 + 4\sin^2\theta_W)(\varepsilon_{\alpha\beta}^{eP})_{NC}N_e \quad (8)$$

where the NSI couplings affecting the CC and NC processes should in principle be distinguished.

---

<sup>1</sup>All expressions are divided by 2 to account for the fact that the medium is unpolarized.

Using equation (2) and the additivity of the quark-current vertices, one gets for the neutrino interaction potential with protons

$$V_p(NSI) = \frac{g_L^2}{2m_W^2} \left[ \varepsilon_{\alpha\beta}^{uP} - \frac{\varepsilon_{\alpha\beta}^{dP}}{2} - \left( \frac{4}{3} 2\varepsilon_{\alpha\beta}^{uP} - \frac{2}{3} 2\varepsilon_{\alpha\beta}^{dP} \right) \sin^2\theta_W \right] N_e. \quad (9)$$

Similarly for neutrons

$$V_n(NSI) = \frac{g_L^2}{2m_W^2} \left( \frac{\varepsilon_{\alpha\beta}^{uP}}{2} - \varepsilon_{\alpha\beta}^{dP} \right) N_n. \quad (10)$$

In both (9) and (10) only neutral currents are involved.

Adding (7), (8), (9) and (10) and dividing by 2 one finally gets

$$V(NSI) = G_F \sqrt{2} N_e \left[ (\varepsilon_{\alpha\beta}^{eP})_{CC} + \left( -\frac{1}{2} + 2\sin^2\theta_W \right) (\varepsilon_{\alpha\beta}^{eP})_{NC} + \left( 1 - \frac{8}{3}\sin^2\theta_W + \frac{N_n}{2N_e} \right) \varepsilon_{\alpha\beta}^{uP} + \left( -\frac{1}{2} + \frac{2}{3}\sin^2\theta_W - \frac{N_n}{N_e} \right) \varepsilon_{\alpha\beta}^{dP} \right] \quad (11)$$

so that the full interaction potential is the sum of eqs.(6) and (11).

In the case of the standard interactions, the interaction potentials for  $\nu_e$  and  $\nu_\alpha$  constitute a diagonal matrix because they cannot be responsible for flavour change [eq.(6)]. This may occur as a consequence of the vacuum mixing angle (oscillations) [25, 26] or the magnetic moment for instance [27, 28]. On the other hand, in the case of NSI the interaction potentials [eq.(11)] constitute a full matrix in neutrino flavour space.

In order to obtain the matter Hamiltonian eqs.(6) and (11) must now be added. In the flavour basis this is

$$\mathcal{H}_M = V_c \begin{pmatrix} 1 & 0 & 0 \\ 0 & 0 & 0 \\ 0 & 0 & 0 \end{pmatrix} + \begin{pmatrix} v_{ee}(NSI) & v_{e\mu}(NSI) & v_{e\tau}(NSI) \\ v_{\mu e}(NSI) & v_{\mu\mu}(NSI) & v_{\mu\tau}(NSI) \\ v_{\tau e}(NSI) & v_{\tau\mu}(NSI) & v_{\tau\tau}(NSI) \end{pmatrix} \quad (12)$$

where in the first term, describing the standard interactions, the additive quantity  $V_n$  which is proportional to the identity, has been removed from the diagonal. In the second term  $v_{\alpha\beta}$  ( $\alpha, \beta = e, \mu, \tau$ ) denote the matrix elements of the interaction potential matrix (11). Finally in the mass basis

$$\mathcal{H} = \begin{pmatrix} 0 & 0 & 0 \\ 0 & \frac{\Delta m_{21}^2}{2E} & 0 \\ 0 & 0 & \frac{\Delta m_{31}^2}{2E} \end{pmatrix} + U^\dagger \mathcal{H}_M U \quad (13)$$

where  $U$  is the PMNS matrix [45]<sup>2</sup>,  $E$  is the neutrino energy and  $\Delta m_{ij}^2 = m_i^2 - m_j^2$  with  $m_i$  ( $i = 1, 2, 3$ ) the neutrino mass. Upon insertion of this Hamiltonian expression in the neutrino evolution equation, the survival ( $P_{ee}$ ) and conversion probabilities ( $P_{e\mu}, P_{e\tau}$ ) are evaluated using the Runge-Kutta numerical integration.

---

<sup>2</sup>We use the standard parameterization [46] for the  $U$  matrix and the central value  $\sin\theta_{13} = 0.13$  claimed in ref. [25].

## 2.2 Neutrino electron scattering detection rates

For the detection in SuperKamiokande and SNO through  $\nu_\alpha e^- \rightarrow \nu_\beta e^-$  scattering, the NSI information comes in the probabilities and the cross section

$$\frac{d\sigma}{dT} = \frac{2G_F^2 m_e}{\pi} \left[ \tilde{g}_L^2 + \tilde{g}_R^2 \left(1 - \frac{T}{E_\nu}\right)^2 - \tilde{g}_L \tilde{g}_R \frac{m_e T}{E_\nu^2} \right] \quad (14)$$

where  $\tilde{g}_{L,R}$  are the  $g_{L,R}$  couplings modified according to [11]<sup>3</sup>

$$\begin{aligned} (\tilde{g}_{L,R})_{\nu_e}^2 &= |(g_{L,R})_{\nu_e}^2 + \varepsilon_{ee}^{e L,R}| + \sum_{\alpha \neq e} |\varepsilon_{\alpha e}^{e L,R}| & \text{for } \nu_e e^- \rightarrow \nu_\alpha e^- \\ (\tilde{g}_{L,R})_{\nu_\mu}^2 &= |(g_{L,R})_{\nu_\mu}^2 + \varepsilon_{\mu\mu}^{e L,R}| + \sum_{\alpha \neq \mu} |\varepsilon_{\alpha\mu}^{e L,R}| & \text{for } \nu_\mu e^- \rightarrow \nu_\alpha e^- \\ (\tilde{g}_{L,R})_{\nu_\tau}^2 &= |(g_{L,R})_{\nu_\tau}^2 + \varepsilon_{\tau\tau}^{e L,R}| + \sum_{\alpha \neq \tau} |\varepsilon_{\alpha\tau}^{e L,R}| & \text{for } \nu_\tau e^- \rightarrow \nu_\alpha e^- . \end{aligned}$$

with  $\alpha = e, \mu, \tau$ .

For  $\nu_e$  both charged and neutral currents are possible, so that

$$(g_L)_{\nu_e} = \frac{1}{2} + \sin^2\theta_W, \quad (g_R)_{\nu_e} = \sin^2\theta_W \quad (15)$$

whereas  $\nu_{\mu,\tau}$  only interact through neutral currents, hence

$$(g_L)_{\nu_\mu, \nu_\tau} = -\frac{1}{2} + \sin^2\theta_W, \quad (g_R)_{\nu_\mu, \nu_\tau} = \sin^2\theta_W. \quad (16)$$

These expressions are then inserted in the spectral event rate

$$R_{SK,SNO}^{th}(E_e) = \frac{\int_{m_e}^{E'_{max}} dE'_e f(E'_e, E_e) \int_{E_m}^{E_M} dE \phi(E) \left[ P_{ee}(E) \frac{d\sigma_e}{dT'} + P_{e\mu}(E) \frac{d\sigma_\mu}{dT'} + P_{e\tau}(E) \frac{d\sigma_\tau}{dT'} \right]}{\int_{m_e}^{E'_{max}} dE'_e f(E'_e, E_e) \int_{E_m}^{E_M} dE \phi(E) \frac{d\sigma_e}{dT'}} \quad (17)$$

which will be evaluated in the next section. Here  $\phi(E)$  denotes the neutrino flux from Boron and hep neutrinos,  $f(E'_e, E_e)$  is the energy resolution function for SuperKamiokande and SNO [47, 48] and the rest of the notation is standard.

Notice that whereas the Hamiltonian (13) is symmetric under the interchange

$$\varepsilon_{\alpha\beta}^L \leftrightarrow \varepsilon_{\alpha\beta}^R \quad \text{for } e, u, d$$

such is not the case for the detection process [see eqs.(14)-(16)]. We finally note that at the detection level the NSI couplings  $\varepsilon_{\alpha\beta}^{L,R}$  are considered separately, as clearly seen from eq.(14), whereas at the level of propagation, since the diagrams involved in the interaction potentials add up, their sum should instead be considered.

<sup>3</sup>This modification is different from the one in ref. [11] since each  $\varepsilon$  coupling as defined in section 2 pertains not to a single vertex but to a whole NSI diagram.

### 3 NSI couplings, probabilities and spectra

We now perform an investigation of the effect of the NSI couplings  $\varepsilon_{\alpha\beta}^{e,u,d} = |\varepsilon_{\alpha\beta}^{e,u,d}| e^{i\phi_{\alpha\beta}^{e,u,d}}$  on the neutrino probability and event rates. Our aim in this section is to find those couplings which lead to a flat SuperKamiokande spectral rate, thus improving the fit with respect to its LMA prediction while keeping the quality of the other solar event rate fits. We start by inserting one coupling at a time, first with equal CC and NC couplings, namely  $(\varepsilon_{\alpha\beta}^{eP})_{CC} = (\varepsilon_{\alpha\beta}^{eP})_{NC} = \varepsilon_{\alpha\beta}^{eP}$  (subsection 3.1) and next with  $(\varepsilon_{\alpha\beta}^{eP})_{CC} \neq (\varepsilon_{\alpha\beta}^{eP})_{NC}$  (subsection 3.2). We then extend our analysis to include all diagonal couplings in subsection 3.3. It is found that complex diagonal entries in the NSI Hamiltonian are the only ones that modify the LMA solution.

**3.1**  $(\varepsilon_{\alpha\beta}^{eP})_{CC} = (\varepsilon_{\alpha\beta}^{eP})_{NC} = \varepsilon_{\alpha\beta}^{eP}$

For the sake of clarity we will organize the NSI couplings in three matrices according to whether the charged fermion in the external line is  $e$ ,  $u$ ,  $d$

$$\begin{pmatrix} \varepsilon_{ee}^{e,u,d P} & \varepsilon_{e\mu}^{e,u,d P} & \varepsilon_{e\tau}^{e,u,d P} \\ \varepsilon_{e\mu}^{*e,u,d P} & \varepsilon_{\mu\mu}^{e,u,d P} & \varepsilon_{\mu\tau}^{e,u,d P} \\ \varepsilon_{e\tau}^{*e,u,d P} & \varepsilon_{\mu\tau}^{*e,u,d P} & \varepsilon_{\tau\tau}^{e,u,d P} \end{pmatrix}. \quad (18)$$

Each set of three couplings  $\varepsilon_{\alpha\beta}^{e,u,d P}$  enters in equation (11) in the entry  $v_{\alpha\beta}$  of the interaction potential matrix. Altogether there are 18 couplings with 36 parameters: each matrix of the three in eq.(18) contains 6 independent entries, each with a modulus and a phase. We analyse one coupling at a time, by taking all others zero. We first consider the cases of purely real and imaginary couplings, hence 4 possibilities for each phase

$$\phi_{\alpha\beta}^{e,u,d} = 0, \pi/2, \pi, (3/2)\pi. \quad (19)$$

Motivated by the arguments expound in the introduction we investigate the parameter range  $|\varepsilon_{\alpha\beta}| \in [5 \times 10^{-5}, 5 \times 10^{-2}]$ . We find that

- Off diagonal entries  $\varepsilon_{\alpha\beta}^{e,u,d P}$  ( $\alpha \neq \beta$ ) which contain  $3 \times 3 \times 4 = 36$  possibilities for moduli and phases do not induce any change in the LMA probability, nor any visible change in the rates, either if one or more at a time are inserted.
- Diagonal entries  $\varepsilon_{\alpha\alpha}^{e,u,d P}$ .
  - (a) Real couplings  $\varepsilon_{\alpha\alpha}^{e,u,d P} = \pm |\varepsilon_{\alpha\alpha}^{e,u,d P}|$  ( $3 \times 3 \times 2 = 18$  possibilities) do not change the LMA probability, hence the rates.
  - (b) Imaginary couplings  $\varepsilon_{\alpha\alpha}^{e,u,d P} = \pm i |\varepsilon_{\alpha\alpha}^{e,u,d P}|$  ( $3 \times 3 \times 2 = 18$  possibilities) lead to probabilities which diverge from  $P_{LMA}$  for all  $|\varepsilon_{\alpha\alpha}| > 5 \times 10^{-5}$ . According to the probability shape that is obtained, we group these cases in the following way

	1	2	3
A	$+i \varepsilon_{ee}^e P $	$+i \varepsilon_{\mu\mu}^e P $	$-i \varepsilon_{ee}^e P $
B	$+i \varepsilon_{ee}^u P $	$+i \varepsilon_{\mu\mu}^u P $	$-i \varepsilon_{ee}^u P $
C	$-i \varepsilon_{ee}^d P $	$-i \varepsilon_{\mu\mu}^d P $	$+i \varepsilon_{ee}^d P $
D	$-i \varepsilon_{\mu\mu}^e P $	$-i \varepsilon_{\tau\tau}^e P $	$+i \varepsilon_{\tau\tau}^e P $
E	$-i \varepsilon_{\mu\mu}^u P $	$-i \varepsilon_{\tau\tau}^u P $	$+i \varepsilon_{\tau\tau}^u P $
F	$+i \varepsilon_{\mu\mu}^d P $	$+i \varepsilon_{\tau\tau}^d P $	$-i \varepsilon_{\tau\tau}^d P $

Table 1: *The NSI couplings that modify the LMA probability.*

All cases in the first column of table 1 along with D2, E2, F2 in the second column lead qualitatively to the same monotonically decreasing probability curve: a high probability ( $P \geq P_{LMA}$ ) for low energy ( $E \lesssim 3 \text{ MeV}$ ) and a low one ( $P \leq P_{LMA}$ ) for intermediate and high energies. The curve becomes increasingly flat in this energy sector as  $\varepsilon_{\alpha\alpha}$  increases, which is also reflected in the flatness of the SuperKamiokande spectral rate. However for cases A1, B1, C1 and D2, E2, F2 the probability gets too high for low energies so that the Ga [49,50] rate fails to be conveniently fitted. The ‘best’ results in the sense that they lead to the most flat spectral rate which approaches the SuperKamiokande one and to a correct fit for Ga are obtained alternatively from cases D1, E1, or F1 for the following values

$$\begin{aligned}
\varepsilon_{\mu\mu}^e P &= -i|\varepsilon_{\mu\mu}^e P| = -i 1.5 \times 10^{-3} \\
\varepsilon_{\mu\mu}^u P &= -i|\varepsilon_{\mu\mu}^u P| = -i 2.5 \times 10^{-3} \\
\varepsilon_{\mu\mu}^d P &= +i|\varepsilon_{\mu\mu}^d P| = +i 2.0 \times 10^{-3}.
\end{aligned} \tag{20}$$

For larger values of the NSI couplings the probability moves further away from its LMA profile so that the Ga rate becomes too high and the  ${}^8\text{B}$  one too low. In fig.1 we plot several survival probabilities: the dashed line is the vacuum one, then at the lowest energy and from bottom to top the first curve is the LMA one, the next corresponds to all cases in (20) and leads to the best fit of the four, the next one to the case  $\varepsilon_{\mu\mu}^e P = -i 3 \times 10^{-3}$  and the top one to  $\varepsilon_{ee}^e P = +i 5 \times 10^{-3}$ . A comparison is shown in table 2 between the predictions and the quality of the fits obtained from LMA and the case  $\varepsilon_{\mu\mu}^e P = -i 1.5 \times 10^{-3}$ . In figs.2 and 3 we show the SuperKamiokande spectrum for LMA (upper curves) and for the first case in (20) (lower curves) superimposed on the data points taken respectively from refs. [29] and [30]. The improvement obtained through the NSI coupling is clearly visible. In fig.4 the two curves are superimposed on the SNO data points for electron scattering [51]. Here the data are also clearly consistent with a constant rate.

The first set of cases in the second column of table 1, namely A2, B2, C2, lead qualitatively to the inverse behaviour with energy of the LMA probability. As  $|\varepsilon_{\alpha\alpha}|$  increases from its lower bound, one gets  $P \leq P_{LMA}$  for low energies ( $E \lesssim 2 - 3 \text{ MeV}$ ) and  $P \geq P_{LMA}$  for intermediate and high energies, so that the fits worsen with respect to the LMA ones.

Furthermore all cases in the third column of table 1, namely A3, B3, C3, D3, E3, F3 lead to probability curves which are totally unsuitable: they deviate drastically from both



	Ga	Cl	SK	SNO <sub>NC</sub>	SNO <sub>CC</sub>	SNO <sub>ES</sub>	$\chi^2_{rates}$	$\chi^2_{SK_{sp}}$	$\chi^2_{SNO}$	$\chi^2_{gl}$
LMA	64.9	2.84	2.40	5.47	1.79	2.37	0.67	42.0	48.6	91.3
$-i \varepsilon_{\mu\mu}^{eP} $	69.7	2.74	2.23	5.47	1.68	2.26	0.11	40.3	45.0	85.4

Table 2: Comparison between the LMA predictions for solar event rates and the NSI ones with  $-i|\varepsilon_{\mu\mu}^{eP}| = -i 1.5 \times 10^{-3}$ . For details of the  $\chi^2$  analysis see for instance [27].

$P_{LMA}$  and a from flat, suitable profile able to generate the SuperKamiokande spectrum.

We have also checked that combinations of real and imaginary parts for all couplings do not change the previous results. This should be expected since, as mentioned earlier, purely real couplings do not change the LMA probability. The only consequence of introducing real parts in the NSI couplings comes in the spectral event rates through the quantities  $\tilde{g}_{L,R}$  in eqs.(14) and (15), but the differences lie much beyond the experimental accuracy.

### 3.2 $(\varepsilon_{\alpha\beta}^{eP})_{CC} \neq (\varepsilon_{\alpha\beta}^{eP})_{NC}$

The analysis of the more general case of different CC and NC couplings affecting the  $\nu_e e$  scattering diagrams can be made quite simple if one examines the coefficients of  $(\varepsilon_{\alpha\beta}^{eP})_{CC}$  and  $(\varepsilon_{\alpha\beta}^{eP})_{NC}$  in eq.(11). The first is unity whereas for equal CC and NC couplings it is 0.96 and the second is now -0.04 as compared to the previous value 0.96 as well. Consequently one expects that the analysis for  $(\varepsilon_{\alpha\beta}^{eP})_{CC}$  leads to approximately the same results as for equal couplings while the results are modified by a factor of 0.96/(-0.04) in the analysis for  $(\varepsilon_{\alpha\beta}^{eP})_{NC}$ . Indeed the convenient modification in the LMA probability is obtained for

$$(\varepsilon_{\mu\mu}^{eP})_{CC} = -i(|\varepsilon_{\mu\mu}^{eP}|)_{CC} = -i 1.4 \times 10^{-3} \quad (21)$$

or alternatively

$$(\varepsilon_{\mu\mu}^{eP})_{NC} = +i(|\varepsilon_{\mu\mu}^{eP}|)_{NC} = +i 3.6 \times 10^{-2}. \quad (22)$$

which lead to the same probability as the cases listed in eq.(20). The results for the other couplings involving u and d quarks are of course unchanged. As before we have considered one coupling at a time to be non zero.

### 3.3 All diagonal couplings

We now allow for all diagonal entries of the NSI term in eq.(12) to be nonzero and complex. In a first step to this generalization we start with all three couplings  $\varepsilon_{\mu\mu}^{e,u,d}$  nonzero simultaneously. Starting with the three equal in moduli, we find that the right modification of the LMA probability is obtained with

$$\begin{aligned} \varepsilon_{\mu\mu}^{eP} &= -i|\varepsilon_{\mu\mu}^{eP}| = -i 0.7 \times 10^{-3} \\ \varepsilon_{\mu\mu}^{uP} &= -i|\varepsilon_{\mu\mu}^{uP}| = -i 0.7 \times 10^{-3} \\ \varepsilon_{\mu\mu}^{dP} &= +i|\varepsilon_{\mu\mu}^{dP}| = +i 0.7 \times 10^{-3}. \end{aligned} \quad (23)$$

In a second step we allow for one diagonal entry in the NSI term of (12) in addition to  $\varepsilon_{\mu\mu}^{e,u,d}$  to be nonzero and complex. We find that a finite  $\varepsilon_{\tau\tau}^{e,u,d}$  as added to the parameter choice (23) leads to a ‘wrong’ probability, unless  $|\varepsilon_{\tau\tau}^{e,u,d}| \lesssim |(1/100)\varepsilon_{\mu\mu}^{e,u,d}|$  in which case the LMA solution remains unchanged. The same is true for  $\varepsilon_{ee}^{e,u,d} \neq 0$ . However adding both  $\varepsilon_{ee}^{e,u,d}$  and  $\varepsilon_{\tau\tau}^{e,u,d}$  to (23), the correct change in the LMA probability can be obtained provided  $|\varepsilon_{ee}^{e,u,d}|$  and  $|\varepsilon_{\tau\tau}^{e,u,d}| \simeq |(1/10)\varepsilon_{\mu\mu}^{e,u,d}|$ . To this end two choices are possible: either the signs of  $\varepsilon_{ee}^{e,u,d}$  are changed with respect to those of table 1 with those of  $\varepsilon_{\tau\tau}^{e,u,d}$  unchanged that is

$$\varepsilon_{ee}^e = -i|\varepsilon_{ee}^e|, \quad \varepsilon_{ee}^u = -i|\varepsilon_{ee}^u|, \quad \varepsilon_{ee}^d = +i|\varepsilon_{ee}^d| \quad (24)$$

and

$$\varepsilon_{\tau\tau}^e = -i|\varepsilon_{\tau\tau}^e|, \quad \varepsilon_{\tau\tau}^u = -i|\varepsilon_{\tau\tau}^u|, \quad \varepsilon_{\tau\tau}^d = +i|\varepsilon_{\tau\tau}^d| \quad (25)$$

or vice-versa.

A solution with all nine diagonal couplings having equal moduli is also possible. It corresponds to

$$|\varepsilon_{ee}^{e,u,d}| \simeq |\varepsilon_{\mu\mu}^{e,u,d}| \simeq |\varepsilon_{\tau\tau}^{e,u,d}| = (2-4) \times 10^{-4} \quad (26)$$

provided the signs of  $\varepsilon_{ee}^{e,u,d}$  are unchanged with respect to table 1 and those of  $\varepsilon_{\tau\tau}^{e,u,d}$  are reversed that is

$$\varepsilon_{ee}^e = +i|\varepsilon_{ee}^e|, \quad \varepsilon_{ee}^u = +i|\varepsilon_{ee}^u|, \quad \varepsilon_{ee}^d = -i|\varepsilon_{ee}^d| \quad (27)$$

and

$$\varepsilon_{\tau\tau}^e = +i|\varepsilon_{\tau\tau}^e|, \quad \varepsilon_{\tau\tau}^u = +i|\varepsilon_{\tau\tau}^u|, \quad \varepsilon_{\tau\tau}^d = -i|\varepsilon_{\tau\tau}^d|. \quad (28)$$

Notice that the reverse choice in signs with respect to (27) and (28) would leave the LMA solution unchanged.

In this section we have analysed the conditions to be imposed on the NSI couplings in order to obtain a suitable survival probability for a flat SuperKamiokande spectrum, an improved Cl rate prediction relative to the LMA one and accurate predictions for all other rates. As shall be seen next, these conditions while necessary, are not sufficient, owing to the fact that neutrino decay in solar matter follows as a consequence of the imaginary diagonal couplings in the Hamiltonian.

## 4 Neutrino decay in solar matter?

We recall that a stable stationary state solution of the wave function, for a particle of energy  $E$ , contains a phase factor  $e^{-iEt}$ . If the Hamiltonian has complex eigenvalues this phase factor becomes instead

$$e^{-i(E-i\Gamma)t} \quad (29)$$

so the state is unstable, with decay rate  $\Gamma$  and lifetime  $\Gamma^{-1}$ .

Since the suitable Hamiltonian that reduces the tension between the LMA solution and the data has imaginary diagonal couplings, its eigenvalues are complex which implies the

existence of unstable states with a finite decay rate. We note that this instability is induced by the solar matter density [see eq.(12)] and in its absence, in the vacuum, the neutrinos are stable. Furthermore, as the number of neutrinos (or neutrinos and antineutrinos) must remain constant as a consequence of unitarity, we must look for those solutions of the wave equation in which at least one but no more than two eigenvalues have a negative imaginary part. The remainder will have positive imaginary parts. This will ensure that the unstable state or states decay into any of the lighter. The negative imaginary parts correspond to the decaying states as it follows from (29), while the positive ones to the states into which the former decay. Such criteria must be imposed together with the requirement of consistency with the solar neutrino data, namely a flat SK spectrum and accurate Ga, Cl and SNO rates. To this end the correct solution is found to be

$$\mathcal{H}_{NSI} = G_F \sqrt{2} N_e \left[ x_1 \begin{pmatrix} \frac{i}{2}\varepsilon & & \\ & -i\varepsilon & \\ & & \frac{i}{2}\varepsilon \end{pmatrix} + x_2 \begin{pmatrix} \frac{i}{2}\varepsilon & & \\ & -i\varepsilon & \\ & & \frac{i}{2}\varepsilon \end{pmatrix} + x_3 \begin{pmatrix} -\frac{i}{2}\varepsilon & & \\ & i\varepsilon & \\ & & -\frac{i}{2}\varepsilon \end{pmatrix} \right] \quad (30)$$

where  $\varepsilon = 3.5 \times 10^{-4}$ . Here

$$x_1 = \frac{1}{2} + 2\sin^2\theta_W, \quad x_2 = 1 - \frac{8}{3}\sin^2\theta_W + \frac{N_n}{2N_e}, \quad x_3 = -\frac{1}{2} + \frac{2}{3}\sin^2\theta_W - \frac{N_n}{N_e} \quad (31)$$

Notice that (30) is consistent with (26), (27) and (28).

In fig.5 (panels (a) and (b)) we plot the real and imaginary parts of the eigenvalues of the Hamiltonian (12) with the solution (30) for the NSI term as a function of the solar fractional radius for a typical solar neutrino energy  $E = 1 \text{ MeV}$ . From panel (b) which displays the imaginary parts, it is seen that a significant decay of one of the mass matter eigenstates can occur during the first 30-40% of the trajectory with an average decay rate  $O(10^{-16} \text{ eV})$ . Further along the neutrinos appear to be stable while still in the sun and in the vacuum. As expected, the decaying state (the negative values in panel (b)) corresponds to the largest of the mass matter eigenstates (panel (a)).

The neutrino decay modes considered in the literature involve photon or majoron emission along with a neutrino or antineutrino. Although radiative decay is enhanced in a medium [52], for the sun such an enhancement is far too small, as it leads to a lifetime at least five orders of magnitude larger than the age of the universe, so such an effect is totally irrelevant here. The same holds for the ‘neutrino spin-light’ in matter [53, 54]. We are therefore left with the possibility of neutrino decay in matter into an antineutrino and a majoron  $\chi$  [55–58]

$$\nu_i \rightarrow \bar{\nu}_j + \chi \quad (32)$$

where subscripts  $i$  and  $j$  denote mass eigenstates.

In the energy range of interest within the sun the neutrino transition is not matter dominated, hence mass and flavour eigenstates do not coincide. So, having started from the interaction potentials which are flavoured based, a rotation from flavour to mass states in

solar matter is needed in order to obtain the decay rate. However the quantity of interest which can be directly related with experiment is the antineutrino probability at the Earth for a particular flavour, namely  $\bar{\nu}_e$ . To this end the above mentioned rotation must be undone in the vacuum. Thus we will work from now on with flavour based quantities.

The probability of antineutrino appearance for flavour  $\beta$  per unit solar radius is then

$$\frac{dP_{\bar{\nu}_\beta}(E_f)}{dr} = \int_{E_f}^{E_{0max}} \phi(E_0) (1 - e^{-\Gamma(r,E_0)r}) \frac{d\Gamma(r, E_0, E_f)}{dE_f} dE_0. \quad (33)$$

Here  $\phi(E_0)$  is the normalized  ${}^8B$  solar neutrino spectrum [59] with  $E_{0max} = 16.56 \text{ MeV}$  and the factor  $(1 - e^{-\Gamma(r,E_f)r})$  takes into account the neutrino flux reduction. The quantity  $\frac{d\Gamma}{dE_f}$  denotes the differential decay rate per unit antineutrino energy  $E_f$  [55,57]

$$\frac{d\Gamma}{dE_f} = \frac{|g_{\alpha\beta}|^2}{8\pi} \frac{E_0 - E_f}{E_0^2} |V_\alpha(r) - \bar{V}_\beta(r)|(NSI) \quad (34)$$

where  $g_{\alpha\beta}$  are the neutrino-majoron couplings and  $V_\alpha, \bar{V}_\beta$  the neutrino and antineutrino interaction potentials<sup>4</sup>. The energy dependent antineutrino production probability from the decay (32) is therefore

$$P_{\bar{\nu}_\beta}(E_f) = \frac{|g_{\alpha\beta}|^2}{8\pi} \int_{R_i}^{R_S} |V_\alpha(r) - \bar{V}_\beta(r)|(NSI) \int_{E_f}^{E_{0max}} \phi(E_0)(1 - e^{-\Gamma(r,E_0)r}) \frac{E_0 - E_f}{E_0^2} dE_0 dr \quad (35)$$

where  $R_S$  is the solar radius and  $R_i$  is the production point, assumed for simplicity at 5% of  $R_S$  for  ${}^8B$  neutrinos. Upper bounds for the neutrino majoron couplings  $g_{\alpha\beta}$  have been estimated [55,58] and in particular the authors of ref. [58] find

$$\sum_{\alpha} |g_{e\alpha}|^2 < 5.5 \times 10^{-6} \quad (36)$$

of particular interest here, since we will be concerned with  $\bar{\nu}_e$  production for comparison with the Borexino [60] and KamLAND [61] upper bounds on solar  $\bar{\nu}_e$ . The probability (35) is calculated in the interval [57]  $[max\{1/2(V_\alpha - \bar{V}_\beta), -\bar{V}_\beta\}, E_{0max}]$  and the decay (32) requires  $Im(V_\alpha - \bar{V}_\beta) > 0$  with  $V_\alpha, \bar{V}_\beta$  obtained from eqs.(11), (30) and (31)

$$V_e(NSI) = \frac{i}{2} G_F \sqrt{2} (3.5 \times 10^{-4}) N_e \left( 1 - \frac{2}{3} \sin^2 \theta_W + \frac{3N_n}{4N_e} \right) \quad (37)$$

$$V_\mu(NSI) = i G_F \sqrt{2} (3.5 \times 10^{-4}) N_e \left( -1 + \frac{4}{3} \sin^2 \theta_W - \frac{3N_n}{2N_e} \right) \quad (38)$$

$$V_\tau(NSI) = \frac{i}{2} G_F \sqrt{2} (3.5 \times 10^{-4}) N_e \left( 1 - \frac{4}{3} \sin^2 \theta_W + \frac{3N_n}{2N_e} \right). \quad (39)$$

---

<sup>4</sup>Recall that neutrino and antineutrino interaction potentials are symmetric to each other,  $V_\beta = -\bar{V}_\beta$ .

We next evaluate the interaction potentials (37)-(39) throughout the neutrino trajectory in the sun (see fig.6), and analyse the possibilities for neutrino-antineutrino decay in terms of the necessary condition  $Im(V_\alpha - \bar{V}_\beta) > 0$ . To this end, inspection of fig.6 shows that the sums  $V_e - \bar{V}_e$ ,  $V_\tau - \bar{V}_e$  and  $V_\mu - \bar{V}_e$  (the two top curves and the fourth from the top in panel (a)) contribute along the whole trajectory to  $\bar{\nu}_e$  production. Similarly  $\bar{\nu}_\mu$  production is less important, as it can depend only on  $V_e - \bar{V}_\mu$  (fourth line from the top in (a)). Finally  $\bar{\nu}_\tau$  production comes from the contribution of  $V_e - \bar{V}_\tau$  and  $V_\tau - \bar{V}_\tau$  (second and third curves from the top in panel (a)) which are both positive over the whole trajectory. The two bottom curves in panel (a) namely  $V_\mu - \bar{V}_\tau$  (or  $V_\tau - \bar{V}_\mu$ ) and  $V_\mu - \bar{V}_\mu$  are both negative, they refer to  $\nu_\tau$  and  $\nu_\mu$  production and need not concern us here. To summarize, the production of:

- $\bar{\nu}_e$  involves  $V_e - \bar{V}_e$ ,  $V_\tau - \bar{V}_e$  and  $V_\mu - \bar{V}_e$
- $\bar{\nu}_\mu$  involves  $V_e - \bar{V}_\mu$
- $\bar{\nu}_\tau$  involves  $V_e - \bar{V}_\tau$  and  $V_\tau - \bar{V}_\tau$ .

Following these rules and using eq.(35) with the upper limit (36), we represent in fig.7 the upper bound of the energy dependent  $\bar{\nu}_e$  production probability,  $P_{\bar{\nu}_e}(E_f)$ . In panel (a) we use a logarithmic scale and in panel (b) both the LMA probability and  $P_{\bar{\nu}_e}(E_f)$  (inner graph) are shown. The antineutrino probability is seen to be extremely small but grows rapidly as  $E_f$  approaches its lower limit. It decrease fast to zero as  $E_f \rightarrow E_{0max}$ , since fewer neutrinos contribute in the upper energy range.

In order to seek a comparison with the data, we first note that the Borexino upper bound on solar  $\bar{\nu}_e$ , namely  $760 \text{ cm}^{-2}\text{s}^{-1}$ , applies for  $E_{\bar{\nu}_e} > 1.8 \text{ MeV}$  which includes most of the  ${}^8\text{B}$  spectrum [60] and so corresponds in practice to a maximum total probability for  $\bar{\nu}_e$  production [40]

$$P_{\bar{\nu}_e} \leq \frac{760}{5.94 \times 10^6} = 1.3 \times 10^{-4}. \quad (40)$$

We therefore consider the area limited by  $P_{\bar{\nu}_e}(E_f)$  and the two extreme abscissæ  $1.8 \text{ MeV}$  and  $16.56 \text{ MeV}$ , dividing it by the area limited by the unit probability and the same two abscissæ. This ratio gives the total probability for  $\bar{\nu}_e$  production to be compared with (40). We find for the ratio of these two areas

$$7.5 \times 10^{-11} \quad (41)$$

which is within the Borexino bound by 6 orders of magnitude..

The KamLAND collaboration, on the other hand, reports a bound  $370 \text{ cm}^{-2}\text{s}^{-1}$  for  $E_{\bar{\nu}_e} > 8.3 \text{ MeV}$  [61] which corresponds to a probability

$$P_{\bar{\nu}_e} \leq \frac{370}{5.94 \times 10^6 \int_{8.3}^{16.56} \phi(E)dE} = 2.1 \times 10^{-4} \quad (42)$$

whereas for the ratio of the corresponding areas we now get

$$3.3 \times 10^{-12} \tag{43}$$

within the KamLAND bound by 7-8 orders of magnitude. Hence any increase in experimental sensitivity will be unable to reveal a possible solar antineutrino flux produced from NSI.

Finally the full physical process in our model for neutrino propagation and decay through NSI in the sun is represented in fig.8. Equation (12) we used for the Hamiltonian does not take into account the extra physics involved in the majoron coupling and is therefore a truncated Hamiltonian, whose hermiticity is restored once the detailed majoron emission process is taken into account.

## 5 Conclusions

We have investigated the prospects for improving the LMA predictions for solar neutrino event rates with NSI. At present there is no evidence of any new physics associated to a scale not too far above the electroweak scale, hence the great variety of theoretical models available for NSI. In our approach we assumed that NSI are extra contributions to the vertices  $\nu_\alpha\nu_\beta$  and  $\nu_\alpha e$ , so the new couplings describe the deviation from the standard model. With this in mind we derived the neutrino interaction potential in solar matter which was added to the standard Hamiltonian, proceeding with the integration of the evolution equation through the Runge-Kutta method. Neutral and charged current couplings are involved in interactions with electrons whereas only neutral couplings affect those with quarks. We considered the new interactions both at the propagation and at the detection level. The improvement we searched for the LMA predictions consisted in finding whether and how the modification induced by NSI can lead to a flat spectral event rate for SuperKamiokande and an event rate for the Cl experiment within  $1\sigma$  of the data, while keeping the accuracy of all other predictions.

We used the current notation for the NSI couplings  $\varepsilon_{\alpha\beta}^{e,u,d P}$  where  $\alpha, \beta$  are the neutrino labels,  $e, u, d$  denote the charged fermion involved in the process and we investigated the range  $|\varepsilon_{\alpha\beta}| \in [5 \times 10^{-5}, 5 \times 10^{-2}]$ . Our most remarkable and intriguing finding is that only the imaginary diagonal couplings in the Hamiltonian provide a solution to the tension between the LMA prediction for the SuperKamiokande spectrum and the data. This implies the existence of unstable neutrino states, the instability being induced by the solar matter. In the vacuum the neutrinos remain stable.

We may now summarize our main results as follows

- Diagonal, imaginary couplings  $\varepsilon_{\alpha\alpha}^{e,u,d P} = \pm i|\varepsilon_{\alpha\alpha}^{e,u,d P}|$  are the only ones that lead to changes of all kinds in the LMA probability and hence the rates.

- Real couplings  $\varepsilon_{\alpha\beta}^{e,u,d P} = \pm|\varepsilon_{\alpha\beta}^{e,u,d P}|$  do not change the LMA probability when considered either one at a time or altogether and thus they induce a small change in the neutrino electron scattering rate ( $\lesssim 1\%$ ) which is far beyond experimental visibility. For the same reason the addition of real parts to the imaginary couplings does not change the results.
- Off diagonal couplings  $\varepsilon_{\alpha\beta}^{e,u,d P}$  ( $\alpha \neq \beta$ ) whether real or imaginary considered either one at a time or altogether do not change the LMA probability and thus the rates in a significant way.
- Solving the tension between the LMA solution and the data, in particular predicting a flat SuperKamiokande spectrum, requires unstable neutrinos, owing to the fact that only imaginary diagonal couplings in the NSI Hamiltonian modify LMA. The requirement of unitarity then gives the following solution

$$\begin{aligned}
\varepsilon_{ee}^{e,u} &= \frac{i}{2}\varepsilon & \varepsilon_{ee}^d &= -\frac{i}{2}\varepsilon \\
\varepsilon_{\mu\mu}^{e,u} &= -i\varepsilon & \varepsilon_{\mu\mu}^d &= i\varepsilon \\
\varepsilon_{\tau\tau}^{e,u} &= \frac{i}{2}\varepsilon & \varepsilon_{\tau\tau}^d &= -\frac{i}{2}\varepsilon
\end{aligned} \tag{44}$$

with  $\varepsilon = 3.5 \times 10^{-4}$ .

- The above facts imply neutrino decay from the heavier to the lighter states in the solar matter probably with majoron emission, since radiative decay is irrelevant in the sun. Having calculated the antineutrino appearance probability, we find however that it is quite unlikely to ever observe experimentally antineutrinos from the sun due to NSI. Small diagonal imaginary NSI couplings lead to quite a small and unobservable antineutrino production probability. However this induces a visible and remarkable change in both the survival and conversion probabilities to  $\nu_\mu$  and  $\nu_\tau$ .
- Experimentally the flatness of the SuperKamiokande and SNO electron energy spectra is at present the only evidence in favour of neutrino NSI in the sun.

Finally the detailed physics involved in majoron emission was not taken into account and the Hamiltonian we used eq.(12) is therefore a truncated one which is sufficient for our purpose.

## Acknowledgments

*We are grateful to Marco Picariello, Luís Lavoura and Sergio Palomares-Ruiz for useful discussions. C. R. Das gratefully acknowledges a scholarship from Fundação para a Ciência e a Tecnologia (FCT, Portugal) ref. SFRH/BPD/41091/2007. This work was partially supported by the Marie Curie RTN MRTN-CT-2006-035505 and by Fundação para a Ciência e a Tecnologia through the projects CERN/FP/109305/2009, PTDC/FIS/098188/2008 and CFTP-FCT UNIT 777 which are partially funded through POCTI (FEDER).*

## References

- [1] M. M. Guzzo, A. Masiero and S. T. Petcov, Phys. Lett. B **260**, 154 (1991).
- [2] E. Roulet, Phys. Rev. D **44**, 935 (1991).
- [3] Y. Grossman, Phys. Lett. B **359**, 141 (1995) [arXiv:hep-ph/9507344].
- [4] L. M. Johnson and D. W. McKay, Phys. Rev. D **61**, 113007 (2000) [arXiv:hep-ph/9909355].
- [5] A. Datta, R. Gandhi, B. Mukhopadhyaya and P. Mehta, Phys. Rev. D **64**, 015011 (2001) [arXiv:hep-ph/0011375].
- [6] P. Huber and J. W. F. Valle, Phys. Lett. B **523**, 151 (2001) [arXiv:hep-ph/0108193].
- [7] P. Huber, T. Schwetz and J. W. F. Valle, Phys. Rev. Lett. **88**, 101804 (2002) [arXiv:hep-ph/0111224].
- [8] T. Ota, J. Sato and N. A. Yamashita, Phys. Rev. D **65**, 093015 (2002) [arXiv:hep-ph/0112329].
- [9] P. Huber, T. Schwetz and J. W. F. Valle, Phys. Rev. D **66**, 013006 (2002) [arXiv:hep-ph/0202048].
- [10] S. Davidson, C. Pena-Garay, N. Rius and A. Santamaria, JHEP **0303**, 011 (2003) [arXiv:hep-ph/0302093].
- [11] J. Barranco, O. G. Miranda, C. A. Moura and J. W. F. Valle, Phys. Rev. D **73**, 113001 (2006) [arXiv:hep-ph/0512195].
- [12] G. Mangano, G. Miele, S. Pastor, T. Pinto, O. Pisanti and P. D. Serpico, Nucl. Phys. B **756**, 100 (2006) [arXiv:hep-ph/0607267].
- [13] S. Antusch, J. P. Baumann and E. Fernandez-Martinez, Nucl. Phys. B **810**, 369 (2009) [arXiv:0807.1003 [hep-ph]].
- [14] C. Biggio, M. Blennow and E. Fernandez-Martinez, JHEP **0903**, 139 (2009) [arXiv:0902.0607 [hep-ph]].
- [15] A. M. Gago, H. Minakata, H. Nunokawa, S. Uchinami and R. Zukanovich Funchal, JHEP **1001**, 049 (2010) [arXiv:0904.3360 [hep-ph]].
- [16] C. Biggio, M. Blennow and E. Fernandez-Martinez, JHEP **0908**, 090 (2009) [arXiv:0907.0097 [hep-ph]].
- [17] C. Wei, Phys. Rev. D **82**, 016008 (2010) [arXiv:1003.1468 [hep-ph]].



- [18] A. Esteban-Pretel, R. Tomas and J. W. F. Valle, Phys. Rev. D **76**, 053001 (2007) [arXiv:0704.0032 [hep-ph]].
- [19] Z. Berezhiani, R. S. Raghavan and A. Rossi, Nucl. Phys. B **638**, 62 (2002) [arXiv:hep-ph/0111138].
- [20] A. Friedland, C. Lunardini and C. Pena-Garay, Phys. Lett. B **594**, 347 (2004) [arXiv:hep-ph/0402266].
- [21] M. M. Guzzo, P. C. de Holanda and O. L. G. Peres, Phys. Lett. B **591**, 1 (2004) [arXiv:hep-ph/0403134].
- [22] O. G. Miranda, M. A. Tortola and J. W. F. Valle, JHEP **0610**, 008 (2006) [arXiv:hep-ph/0406280].
- [23] A. Bolanos, O. G. Miranda, A. Palazzo, M. A. Tortola and J. W. F. Valle, Phys. Rev. D **79**, 113012 (2009) [arXiv:0812.4417 [hep-ph]].
- [24] F. J. Escrivuela, O. G. Miranda, M. A. Tortola and J. W. F. Valle, Phys. Rev. D **80**, 105009 (2009) [Erratum-ibid. D **80**, 129908 (2009)] [arXiv:0907.2630 [hep-ph]].
- [25] G. L. Fogli *et al.*, Phys. Rev. D **78**, 033010 (2008) [arXiv:0805.2517 [hep-ph]].
- [26] T. Schwetz, M. A. Tortola and J. W. F. Valle, New J. Phys. **10**, 113011 (2008) [arXiv:0808.2016 [hep-ph]].
- [27] C. R. Das, J. Pulido and M. Picariello, Phys. Rev. D **79**, 073010 (2009) [arXiv:0902.1310 [hep-ph]].
- [28] J. Pulido, C. R. Das and M. Picariello, J. Phys. Conf. Ser. **203**, 012086 (2010) [arXiv:0910.0203 [hep-ph]].
- [29] S. Fukuda *et al.* (Super-Kamiokande Collaboration), Phys. Lett. B **539**, 179 (2002) [arXiv:hep-ex/0205075].
- [30] J. P. Cravens *et al.* (Super-Kamiokande Collaboration), Phys. Rev. D **78**, 032002 (2008) [arXiv:0803.4312 [hep-ex]].
- [31] Michael B. Smy (Super-Kamiokande Collaboration), J. Phys. Conf. Ser. **203**, 012082 (2010).
- [32] B. T. Cleveland *et al.*, Astrophys. J. **496**, 505 (1998).
- [33] P. C. de Holanda and A. Y. Smirnov, Phys. Rev. D **69**, 113002 (2004) [arXiv:hep-ph/0307266].

- [34] D. Aristizabal Sierra, M. Hirsch and S. G. Kovalenko, Phys. Rev. D **77**, 055011 (2008) [arXiv:0710.5699 [hep-ph]].
- [35] M. Malinsky, J. C. Romao and J. W. F. Valle, Phys. Rev. Lett. **95**, 161801 (2005) [arXiv:hep-ph/0506296].
- [36] F. Bazzocchi, D. G. Cerdeno, C. Munoz and J. W. F. Valle, Phys. Rev. D **81**, 051701 (2010) [arXiv:0907.1262 [hep-ph]].
- [37] M. Malinsky, T. Ohlsson and H. Zhang, Phys. Rev. D **79**, 011301 (2009) [arXiv:0811.3346 [hep-ph]].
- [38] Z. Berezhiani and A. Rossi, Phys. Lett. B **535**, 207 (2002) [arXiv:hep-ph/0111137].
- [39] M. B. Gavela, D. Hernandez, T. Ota and W. Winter, Phys. Rev. D **79**, 013007 (2009) [arXiv:0809.3451 [hep-ph]].
- [40] C. Pena-Garay and A. Serenelli, arXiv:0811.2424 [astro-ph].
- [41] S. Nussinov, Phys. Lett. B **185**, 171 (1987).
- [42] R. S. Raghavan, X. G. He and S. Pakvasa, Phys. Rev. D **38**, 1317 (1988).
- [43] Z. G. Berezhiani and M. I. Vysotsky, Phys. Lett. B **199**, 281 (1987).
- [44] Z. G. Berezhiani and A. Rossi, arXiv:hep-ph/9306278. 5th International Symposium On Neutrino Telescopes, proceedings edited by M. Baldo Ceolin, Padua, Italy, INFN, 1993.
- [45] Z. Maki, M. Nakagawa and S. Sakata, Prog. Theor. Phys. **28**, 870 (1962).
- [46] C. Amsler *et al.* (Particle Data Group), Phys. Lett. B **667**, 1 (2008).
- [47] Y. Fukuda *et al.* (Super-Kamiokande Collaboration), Phys. Rev. Lett. **81**, 1158 (1998) [Erratum-ibid. **81**, 4279 (1998)] [arXiv:hep-ex/9805021].
- [48] B. Aharmim *et al.* (SNO Collaboration), Phys. Rev. C **72**, 055502 (2005) [arXiv:nucl-ex/0502021].
- [49] C. Cattadori, N. Ferrari and L. Pandola, Nucl. Phys. Proc. Suppl. **143**, 3 (2005).
- [50] V. N. Gavrin and B. T. Cleveland, arXiv:nucl-ex/0703012.
- [51] B. Aharmim *et al.* (SNO Collaboration), Phys. Rev. C **81**, 055504 (2010) [arXiv:0910.2984 [nucl-ex]].
- [52] C. Giunti, C. W. Kim and W. P. Lam, Phys. Rev. D **43**, 164 (1991).

- [53] A. Lobanov and A. Studenikin, Phys. Lett. B **601**, 171 (2004) [arXiv:astro-ph/0408026].
- [54] A. Grigoriev, A. Lokhov, A. Studenikin and A. Ternov, arXiv:1003.0630 [hep-ph].
- [55] M. Kachelriess, R. Tomas and J. W. F. Valle, Phys. Rev. D **62**, 023004 (2000) [arXiv:hep-ph/0001039].
- [56] R. Tomas, H. Pas and J. W. F. Valle, Phys. Rev. D **64**, 095005 (2001) [arXiv:hep-ph/0103017].
- [57] Y. Farzan, Phys. Rev. D **67**, 073015 (2003) [arXiv:hep-ph/0211375].
- [58] A. P. Lessa and O. L. G. Peres, Phys. Rev. D **75**, 094001 (2007) [arXiv:hep-ph/0701068].
- [59] John Bahcall's homepage, <http://www.sns.ias.edu/~jnb/>.
- [60] G. Bellini *et al.* (Borexino Collaboration), Phys. Lett. B **696**, 191 (2011) arXiv:1010.0029 [hep-ex].
- [61] K. Eguchi *et al.* (KamLAND Collaboration), Phys. Rev. Lett. **92**, 071301 (2004) [arXiv:hep-ex/0310047].

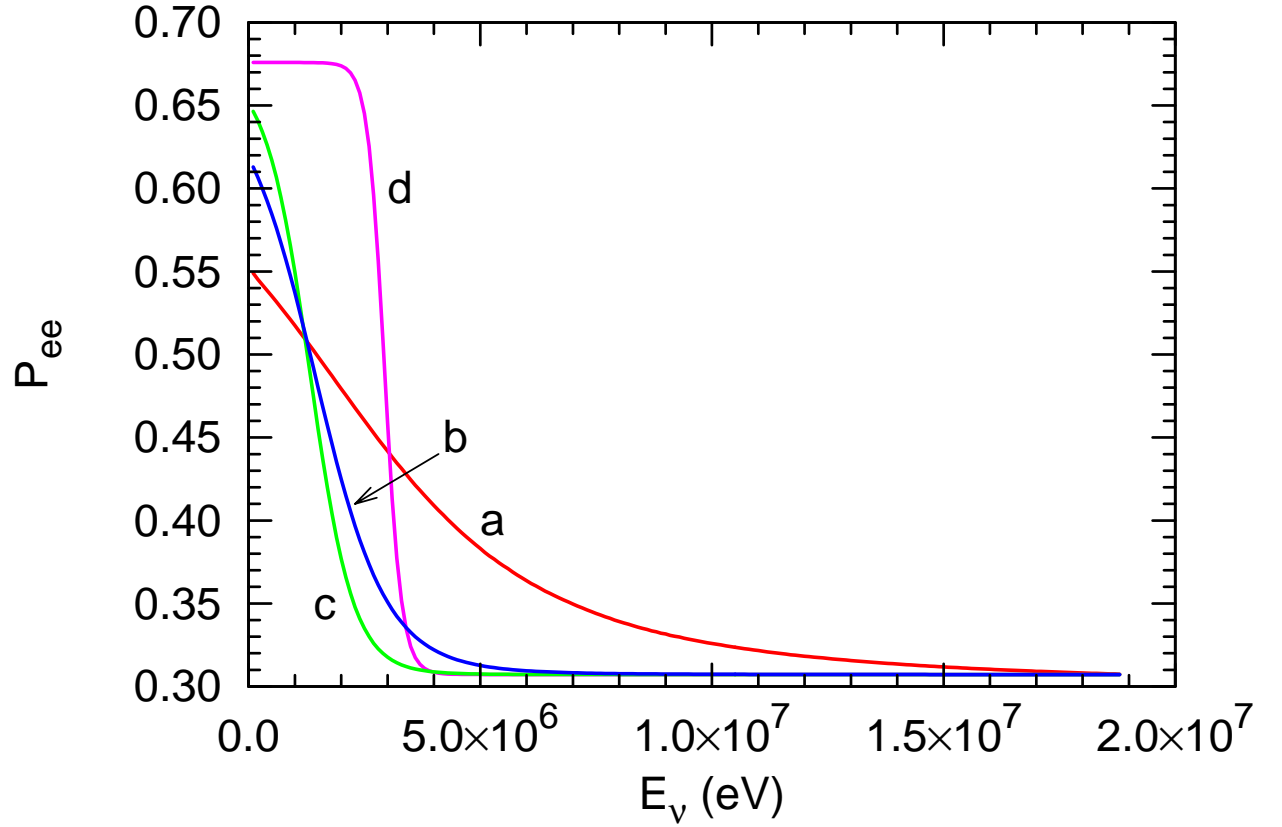


Figure 1: *Survival probabilities as a function of neutrino energy in eV. The dashed line is the vacuum one. The remainder are (a) the LMA one, the one providing the best fit to the data (b) with  $\varepsilon_{\mu\mu}^{eP} = -i 1.5 \times 10^{-3}$  [eq.(20)], curve (c) for  $\varepsilon_{\mu\mu}^{eP} = -i 3 \times 10^{-3}$  and curve (d) for  $\varepsilon_{\mu\mu}^{eP} = +i 5 \times 10^{-3}$  with other non standard couplings vanishing in each case. The last two curves ((c) and (d)) lead to an unacceptably high Ga rate prediction [49, 50].*

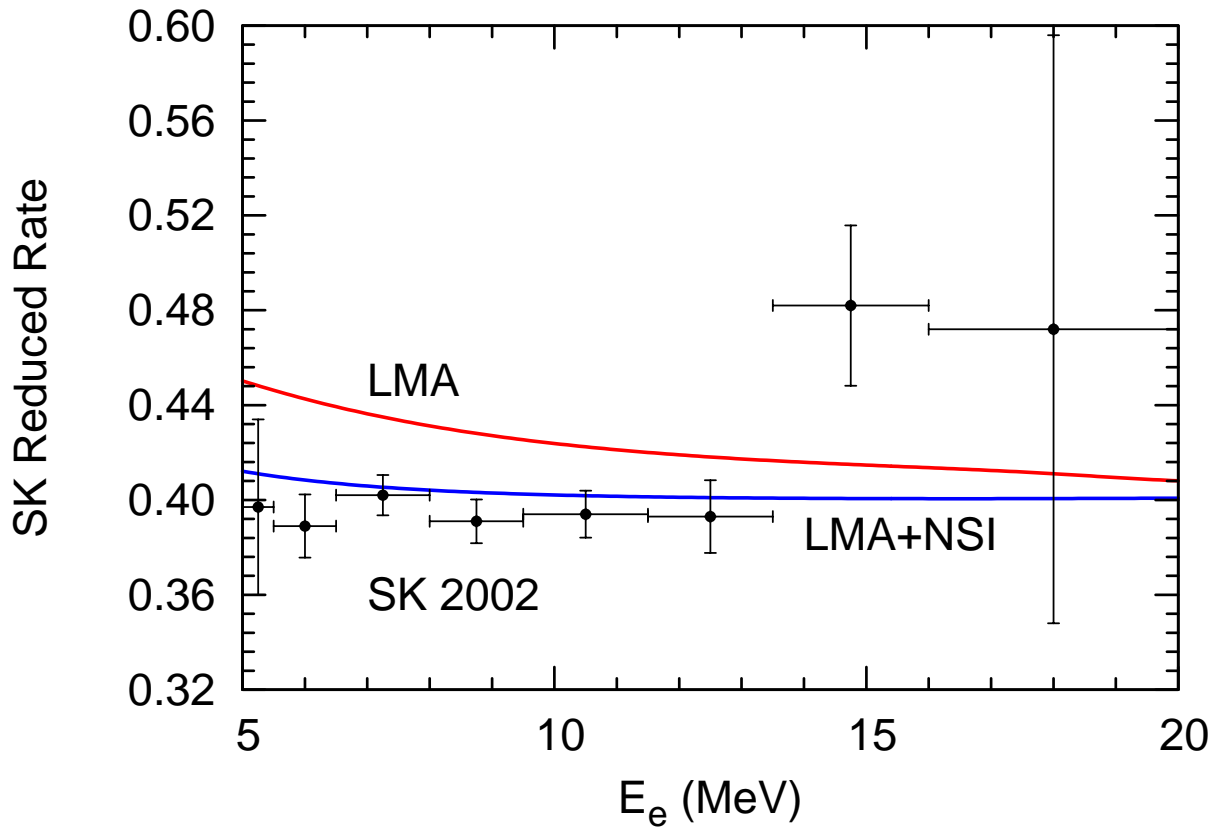


Figure 2: Predictions for SuperKamiokande (units in MeV for electron energy). The upper curve is the LMA spectrum and the lower curve is the LMA spectrum with non standard interactions as in eqs.(23) or (24). These are superimposed on the data published by the Collaboration in 2002 [29].

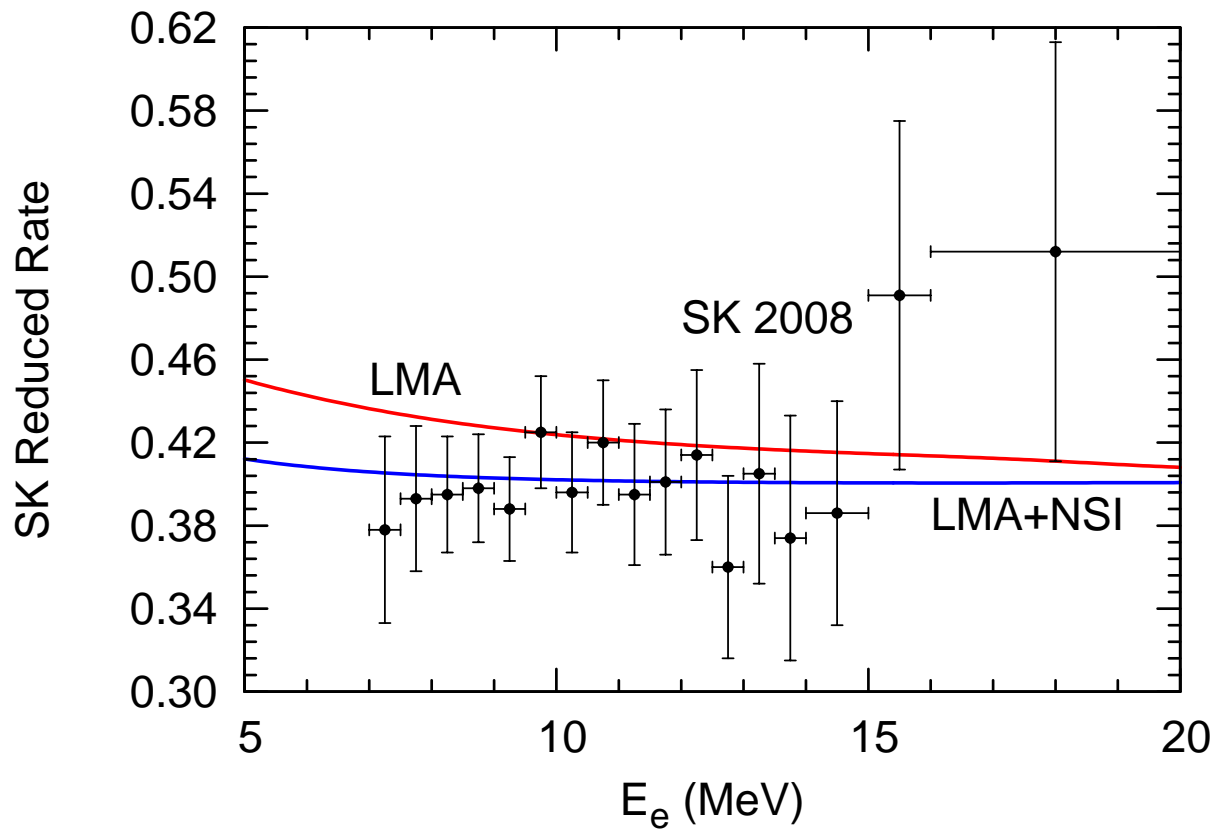


Figure 3: *Same as fig.2 with the data published in 2008 [30].*

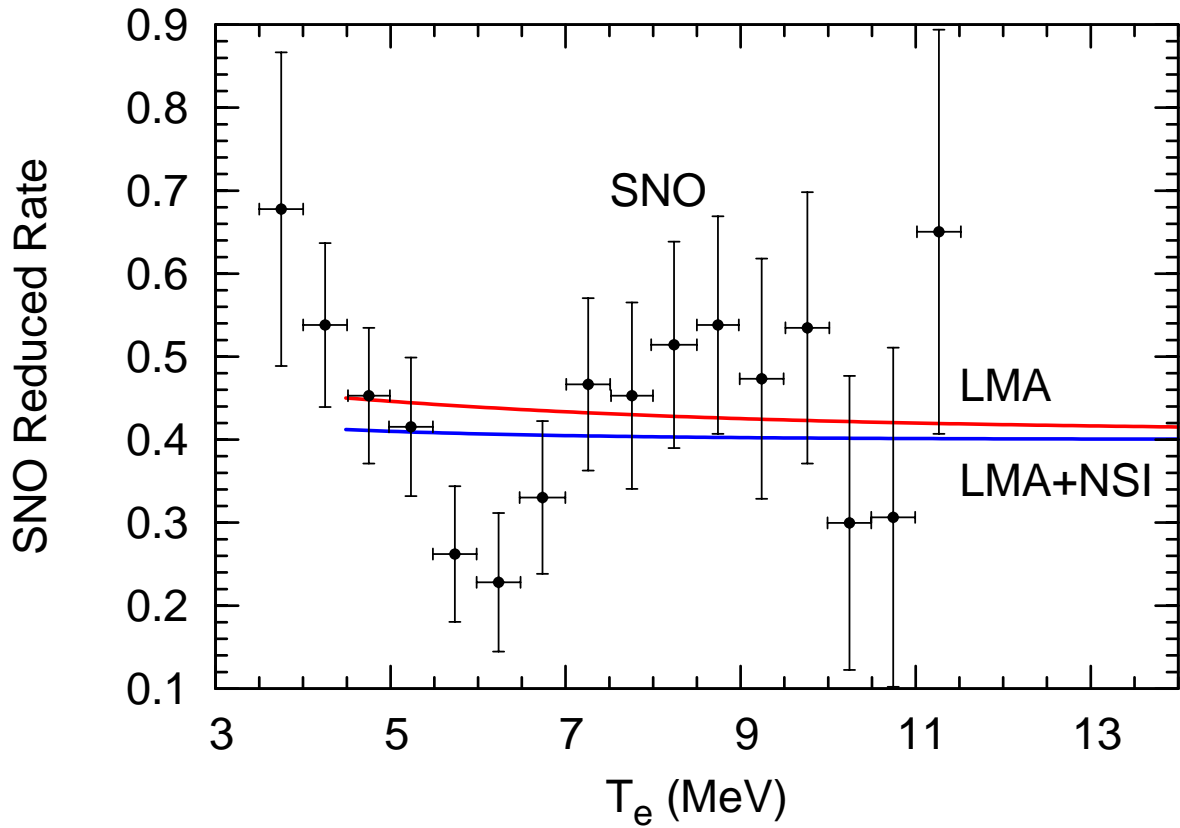


Figure 4: Predictions for SNO neutrino electron scattering superimposed on the data [51] (units in MeV for electron kinetic energy). The upper curve is the LMA prediction and the lower curve is the LMA one with non standard interactions. Error bars are larger than in SuperKamiokande so that the data are consistent with a flat spectrum.

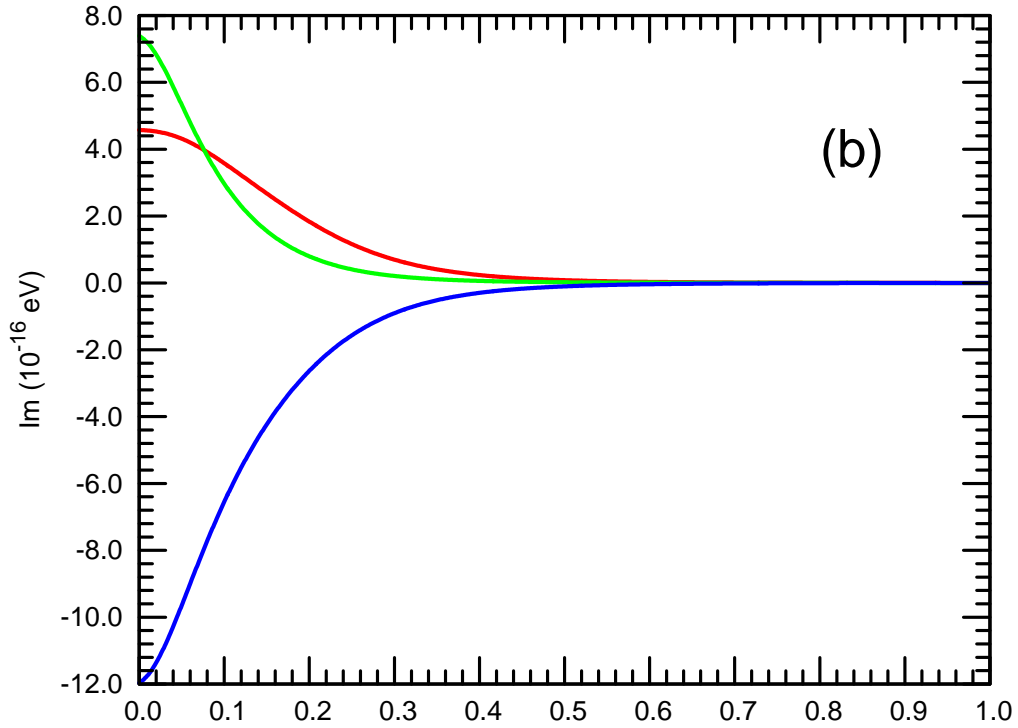
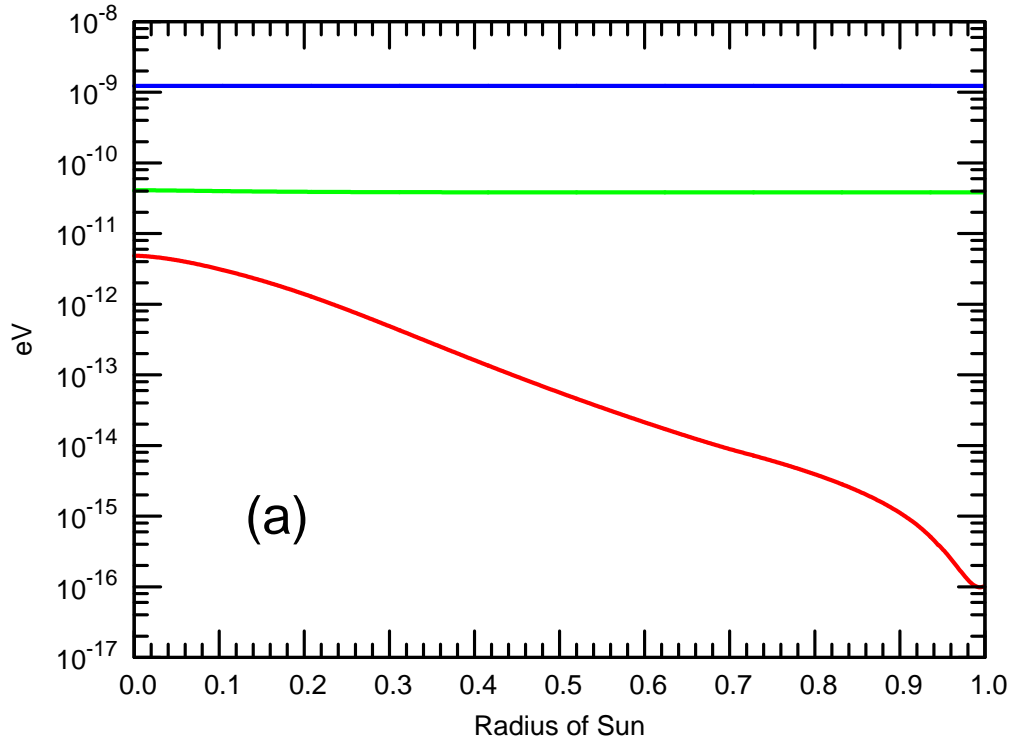


Figure 5: The real (a) and imaginary parts (b) of the neutrino mass matter eigenvalues for  $E = 1$  MeV: the lower curve in (b) associated to the decaying state corresponds to the upper curve in (a), the largest of the mass matter eigenvalues.



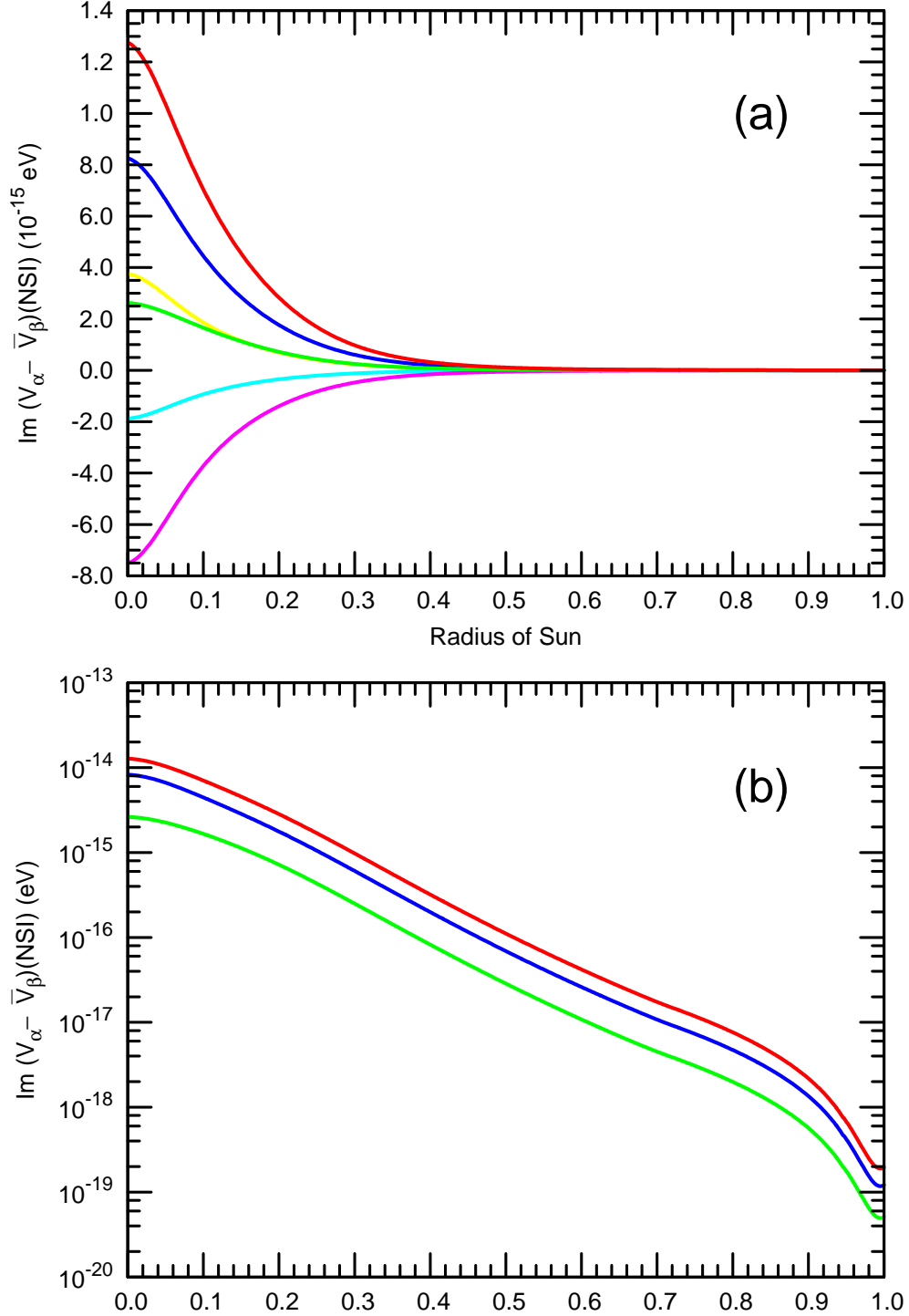


Figure 6: Neutrino NSI potentials along the sun: panel (a) from top to bottom displays the imaginary parts of  $V_e - \bar{V}_e$ ,  $V_e - \bar{V}_\tau$  (or  $V_\tau - \bar{V}_e$ ),  $V_\tau - \bar{V}_\tau$ ,  $V_e - \bar{V}_\mu$  (or  $V_\mu - \bar{V}_e$ ),  $V_\mu - \bar{V}_\tau$  (or  $V_\tau - \bar{V}_\mu$ ) and  $V_\mu - \bar{V}_\mu$ . The first, second and fourth from the top, pertaining to  $\bar{\nu}_e$  production, are also shown in panel (b) in logarithmic scale.

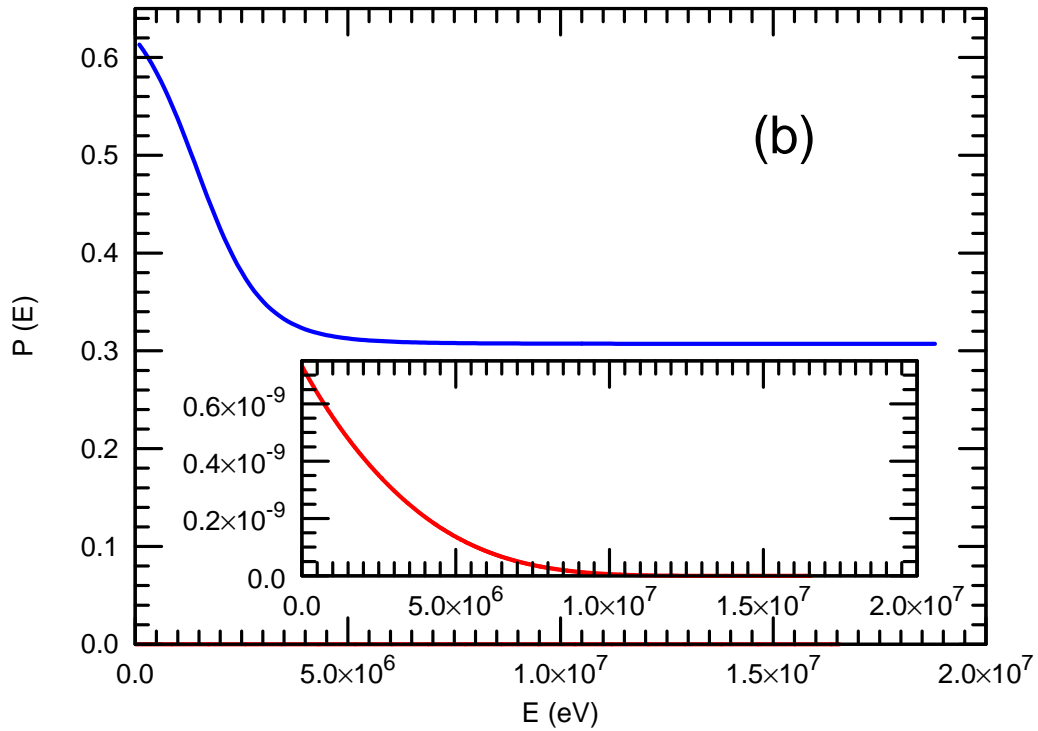
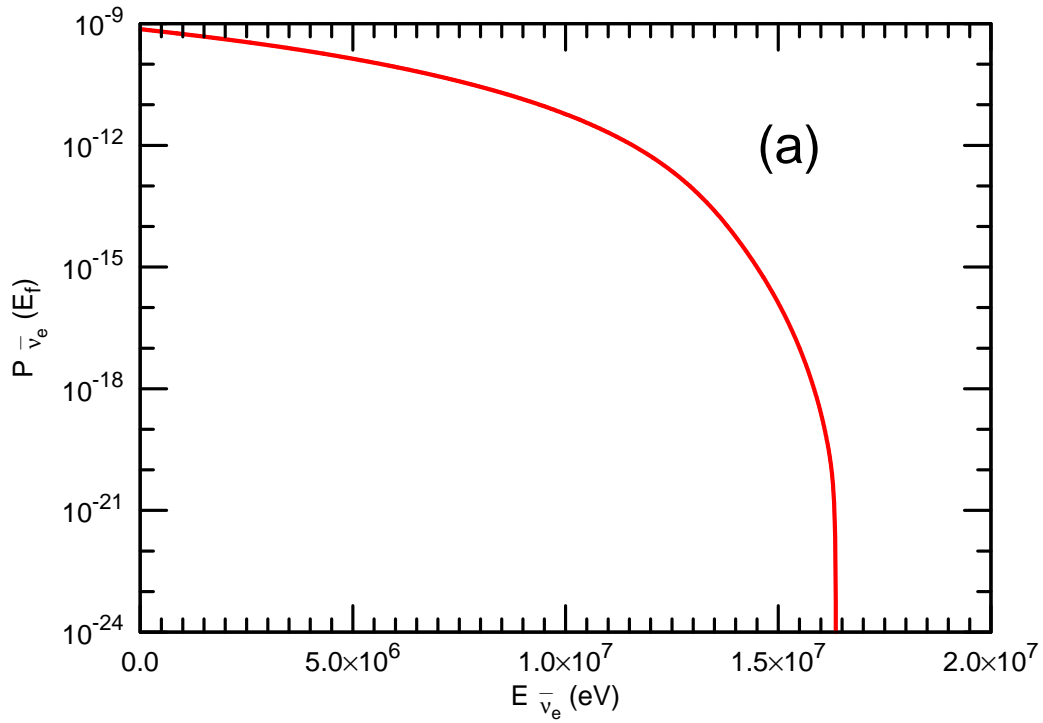


Figure 7: Panel (a): antineutrino production probability in a logarithmic scale. Panel (b): LMA+NSI probability and antineutrino production probability (inner graph). Its extremely small value prevents the possibility of observing antineutrinos from the sun from NSI.

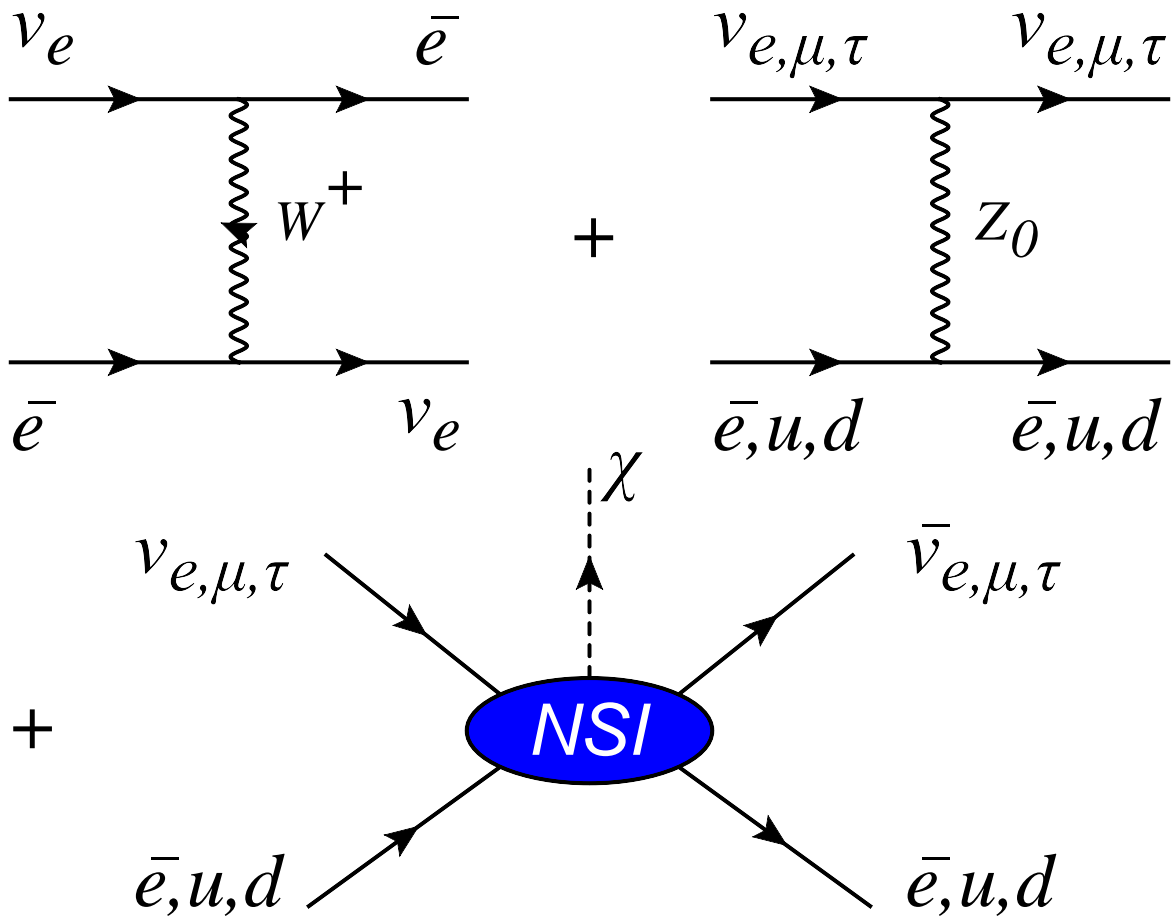


Figure 8: *The processes involved in the propagation of neutrinos in the sun as in our model: the two upper diagrams are the standard ones for matter oscillation and the lower one represents the decay  $\nu_i \rightarrow \bar{\nu}_j + \text{majoron}(\chi)$ .*